C. R. Physique 16 (2015) 836–850

Contents lists available at ScienceDirect

Comptes Rendus Physique

www.sciencedirect.com

Radio science for connecting humans to information systems / L'homme connecté

4G antennas for wireless eyewear devices and related SAR

Antennes 4G pour lunettes connectées et indices DAS associés

Aykut Cihangir [a], Will Whittow [b], Chinthana Panagamuwa [b], Gilles Jacquemod [a], Frédéric Gianesello [c], Cyril Luxey [a,*]

[a] *"Électronique pour Objets Connectés" (EpOC), Université de Nice–Sophia Antipolis, France*
[b] *Wireless Communications Research Group, School of Electronic, Electrical & Systems Engineering, Loughborough University, UK*
[c] *STMicroelectronics, Crolles, France*

ARTICLE INFO

Article history:
Available online 6 November 2015

Keywords:
Eyewear device
Coupling element
LTE
SAR

Mots-clés :
Lunettes connectées
Élément de couplage
LTE
DAS

ABSTRACT

In this paper, we first present a feasibility study to design 4G antennas (700–960 MHz and 1.7–2.7 GHz) for eyewear devices. Those eyewear devices should be connected to the last generation cellular networks, Wireless Local Area Networks or wireless hotspots. Three coupling element type antennas with their matching networks are evaluated in terms of reflection coefficient and total radiation efficiency when the eyewear is placed on the user's head. We also present Specific Absorption Rate (SAR) simulations when the eyewear is positioned over a homogeneous SAM phantom and over a heterogeneous VH (Visible Human) phantom: the SAR levels are compared to international limit values. In a second step, we present experimental results obtained with 3D printed eyewear and coupling elements etched on a classical PCB substrate where the matching circuits are optimized close to the feeding point of the coupling element. Simulated and measured values are in very good agreement: 7 to 16% and 9 to 35% total efficiency are respectively obtained for the low- and high-frequency bands. However, simulated SAR values are somewhat higher than authorized levels with preoccupant high electromagnetic field distribution close to the eye of the user.

RÉSUMÉ

Dans cet article, nous présentons tout d'abord une étude de faisabilité d'antennes 4G (700–960 MHz et 1,7–2,7 GHz) intégrables dans une paire de lunettes connectées. Cet objet est destiné à être connecté aux réseaux de communication cellulaires de dernière génération ainsi qu'aux réseaux personnels de type WLAN. Le concept antennaire d'élément de couplage associé à un circuit d'adaptation est ainsi évalué en termes de coefficient de réflexion et d'efficacité rayonnée lorsque les lunettes sont positionnées sur la tête de l'utilisateur. Nous présentons également l'analyse dosimétrique des prototypes optimisés pour le fantôme homogène SAM et le fantôme évolué hétérogène *Visible Human* (VH) : les niveaux de DAS dans ces deux fantômes sont simulés et comparés aux normes internationales. Dans un second temps, nous présentons les premiers résultats expérimentaux obtenus à partir de prototypes fabriqués par une imprimante 3D pour la monture des lunettes et des procédés de réalisation classique pour les PCB qui accueillent

* Corresponding author.
E-mail addresses: aykut.cihangir@unice.fr (A. Cihangir), W.G.Whittow@lboro.ac.uk (W. Whittow), frederic.gianesello@st.com (F. Gianesello).

http://dx.doi.org/10.1016/j.crhy.2015.10.009
1631-0705/

les éléments de couplage antennaire et leur circuit d'adaptation. Les valeurs théoriques et expérimentales concernant les coefficients de réflexion et les efficacités totales des antennes sont en très bon accord, attestant ainsi une efficacité rayonnée variant de 10 à 12 % en bande basse et de 20 à 35 % en bande haute. Cependant, les simulations dosimétriques révèlent des niveaux de DAS qui peuvent dépasser les normes du fait des fortes efficacités rayonnées obtenues avec les antennes conçues, notamment avec des pics préoccupants observés au niveau de l'œil.

1. Introduction

During the past years, wireless devices like smartphones, watches, tablets, have been growing tremendously. Recently, a strong interest has emerged for eyewear devices. Every major company have on-going research and development on this topic, the most advanced being Google Glass from Google Inc. that have been already launched and recently stopped for being enhanced and for a better understanding of the potential market of those devices [1]. Those first glasses are using the Bluetooth 4.0 and Wi-Fi 802.11b/g protocol standards at 2.4 GHz. The antenna component is placed along the ear of the user like in wireless Bluetooth headsets for smartphones [2,3]. As the involved output power of the front-end-modules of the Bluetooth and WLAN transceivers are relatively low, the Specific Absorption Rate (SAR) is not an issue to be checked [4,5]. The majority of the users who already tried those glasses considered them as really ergonomic and excellent for daily usage, but they also pointed out a strong limitation in terms of connectivity (only Bluetooth and WLAN standards): indeed the user should have his smartphone in close vicinity of the eyewear or he should be located in a wireless hotspot area. In this context, there is clearly a need for the second generation of smart glasses to be connected to the cellular network. Therefore, 4G antennas should be designed for this purpose and SAR aspect should be cautiously studied.

In this paper, we first present a feasibility study (based on [6]) to design 4G antennas (700–960 MHz and 1.7–2.7 GHz) for eyewear devices to be connected to the last generation cellular networks and Wireless Local Area Networks. Three coupling element type antennas with their matching networks are evaluated in terms of reflection coefficient and total radiation efficiency when the eyewear is placed on the user's head. We also present Specific Absorption Rate (SAR) simulations when the eyewear is positioned over a homogeneous SAM phantom and over an heterogeneous VH (Visible Human) phantom: the SAR levels are compared to international limit values. In a second step, we present experimental results obtained with 3D printed eyewear and coupling elements etched on a classical PCB substrate where the matching circuits are optimized close to the feeding point of the coupling element. Simulated SAR values are also given for these optimized prototypes.

2. Feasibility study

2.1. Design of antenna concepts

It is extremely challenging to design a 4G dual-wideband antenna (30 and 45% bandwidth respectively for 700–960 MHz and 1.7–2.7 GHz) considering the small space available in the eyewear platform. As the free space wavelength at 700 MHz is larger than the allocated space for the antenna (42.8 cm versus 2–3 cm), a resonant antenna is absolutely not the adequate choice. We propose to use a coupling element to excite currents over the Printed Circuit Board (PCB) of the eyewear aiming at a lower radiation quality factor than in the case of a resonant antenna and therefore a potentially higher radiation bandwidth [7]. A coupling element is fed like a monopole antenna but the coupling element is optimized to efficiently excite the currents of a metallic body (here the ground plane of the eyewear PCB) instead of a monopole antenna, optimized to resonate and radiate. The input impedance of the coupling element is then adjusted to the desired value, 50 Ω here, with the help of an optimized matching circuit. The PCB we choose is shown in Fig. 1: realistic dimensions have been extracted from [1].

It should be specified at this stage that we considered plastic eyewear only as opposed to metallic ones. However, it has been demonstrated in [8,9] that a metallic frame has non-negligible effects upon the antenna's performance and the SAR values. We sequentially achieved our simulations with the SAM and VH heads. The total dimensions of the FR4 PCB have been set to $160 \times 20 \times 0.8$ mm^3 (see Fig. 1a) with a perpendicular part in front of the eye ($32 \times 20 \times 0.8$ mm^3) and a metal-less part around the ear of the user ($55 \times 15 \times 0.8$ mm^3). Our analysis of the shape of this structure led us to consider three potential positions for the integration of an efficient capacitive coupling element. The first one consists in placing the coupling element in the middle of the long portion of the PCB that is in front of the ear. The coupling element we optimized is a simple metallic strip having a width of 2 mm, printed on the inner surface of the PCB (in front of the SAM phantom). Electromagnetic simulations have been conducted with EMPIRE XCel 6.01 software. The bandwidth potential has been obtained with Optenni Lab software [10] considering a 2-component matching network and a reflection coefficient lower than −6 dB. The blue curve in Fig. 1b is obtained as follows: for every frequency point, Optenni software tries several topologies of matching networks (with optimized component values) to satisfy the criterion we specified (|reflection coefficient| < -6 dB) considering the simulated input impedance of the coupling element as its input data.

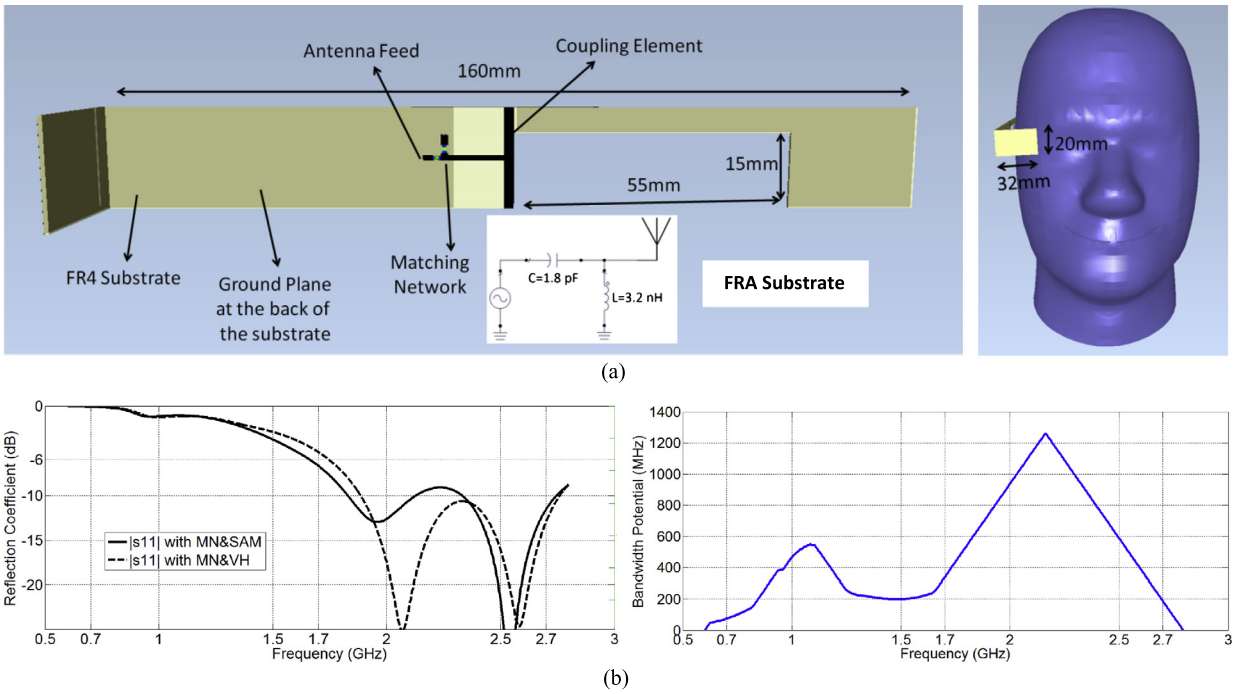

Fig. 1. (Color online.) (a) Prototype 1 optimized with SAM head; (b) simulation results (reflection coefficient and bandwidth potential) for prototype 1 with SAM and VH heads.

The best matching network circuit is kept (highest frequency bandwidth) and the bandwidth potential value is given at this frequency point. This bandwidth potential reveals the frequency bandwidth we should get from this "Coupling Element + Matching Network" considering a reflection coefficient lower than −6 dB.

To satisfy our matching goal, the bandwidth potential should be 260 MHz, centered at 830 MHz and 1 GHz centered at 2.2 GHz. In Fig. 1b, the bandwidth potential is sufficient to cover the high band (higher than 1 GHz), but the low band (700–960 MHz) is not covered. This is mainly due to the fact that the position of the coupling element is not optimal for the excitation of the currents flowing over the PCB. However, we indeed decided to optimize a matching circuit with a shunt inductor (found to be 3.2 nH) and a series capacitor (found to be 1.8 pF) to operate in the 1.7–2.7-GHz band with a reflection coefficient lower than −6 dB. In Fig. 1b, it can be seen that not so much differences exist between the simulated reflection coefficient with SAM head and the reflection coefficient with VH head. The simulated radiation efficiency, which takes into account the losses in the head, ranges from 20 to 25% in the frequency band of interest.

In prototype 2, the coupling element was placed behind the ear (Fig. 2a). The obtained bandwidth potential in low and high bands is definitely higher than the ones obtained with prototype 1 (Fig. 2b). PCB currents are definitely better excited with this coupling element position, as we can benefit from all the length of the available PCB. With a 2-component matching network (a shunt inductor of 14 nH and a series capacitor of 1.6 pF), a dual-band behavior is obtained to ensure operation in the 700–960-MHz and 1.7–2.7-GHz frequency bands, with a reflection coefficient lower than −6 dB. As before, it can be seen that not so much differences exist for the reflection coefficient if we compare the simulated curves with SAM and VH heads. In average, simulated radiation efficiencies are 9% in low band and 20% in high band.

The coupling element from prototype 3 is placed at the end of the frame, in front of the eye (Fig. 3a). Dual-band coverage is obtained with a 3-component matching network (two series inductors being 8 and 12 nH and a shunt capacitor being 0.2 pF). It can be seen again that not so much differences exist for the reflection coefficient if we compare the simulated curves with SAM and VH heads. In average, simulated radiation efficiencies are 14% in low band and 36% in high band.

3D radiation patterns of all three prototypes are shown in Fig. 4 at 800 MHz and 2.2 GHz. All antennas tend to radiate in a direction perpendicular to their coupling elements, away from the user's head as it is usually the case in smartphones. However, it is of paramount importance to simulate the SAR levels generated in SAM and VH heads.

2.2. SAR simulations

During the past twenty years, there has been a strong public and scientific interest for possible harms of radiated electromagnetic waves by mobile phones. The power transmitted by a mobile phone is therefore accurately regulated to limit the absorbed power levels by the user's head. The main characteristic to evaluate the interaction with the user is the SAR: RF power absorbed by a unit mass of tissue (W/kg). Two international limits exist: one in Europe (SAR limited to 2 W/kg averaged over 10 g during 6 min) [11] and one in the USA (SAR limited to 1.6 W/kg averaged over 1 g during

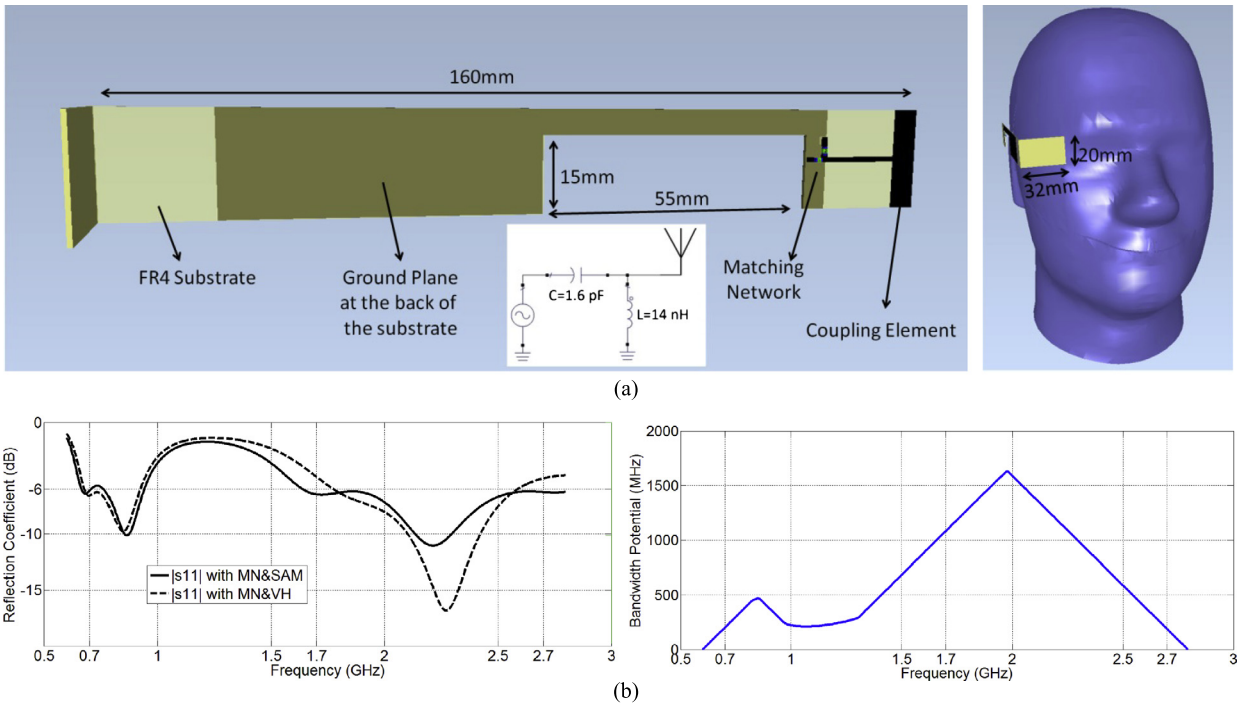

Fig. 2. (Color online.) (a) Prototype 2 optimized with SAM head; (b) simulation results (reflection coefficient and bandwidth potential) for prototype 2 with SAM and VH heads.

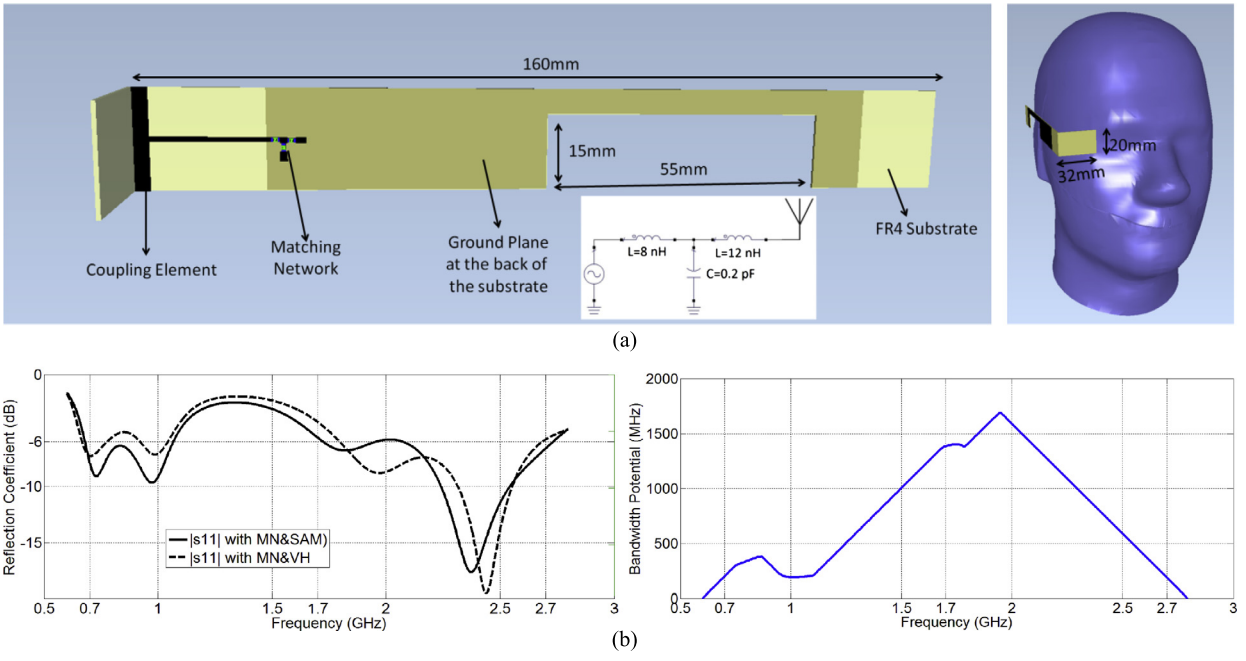

Fig. 3. (Color online.) (a) Prototype 3 optimized with SAM head; (b) simulation results (reflection coefficient and bandwidth potential) for prototype 3 with SAM and VH heads.

30 min [12]). Lots of papers have simulated SAR levels in the user's head originated by a mobile phone when positioned close to homogeneous SAM or heterogeneous VH head phantoms [13,14]. The averaged SAR over 1 g is typically twice the SAR averaged over 10 g. SAM heads usually creates higher SAR values than VH ones. It is well established that the SAR level created by a mobile phone depends on the transmitted frequency, the distance of the electromagnetic source from the head and the antenna type. The SAR value in homogeneous phantom exponentially decreases as we move away from the source.

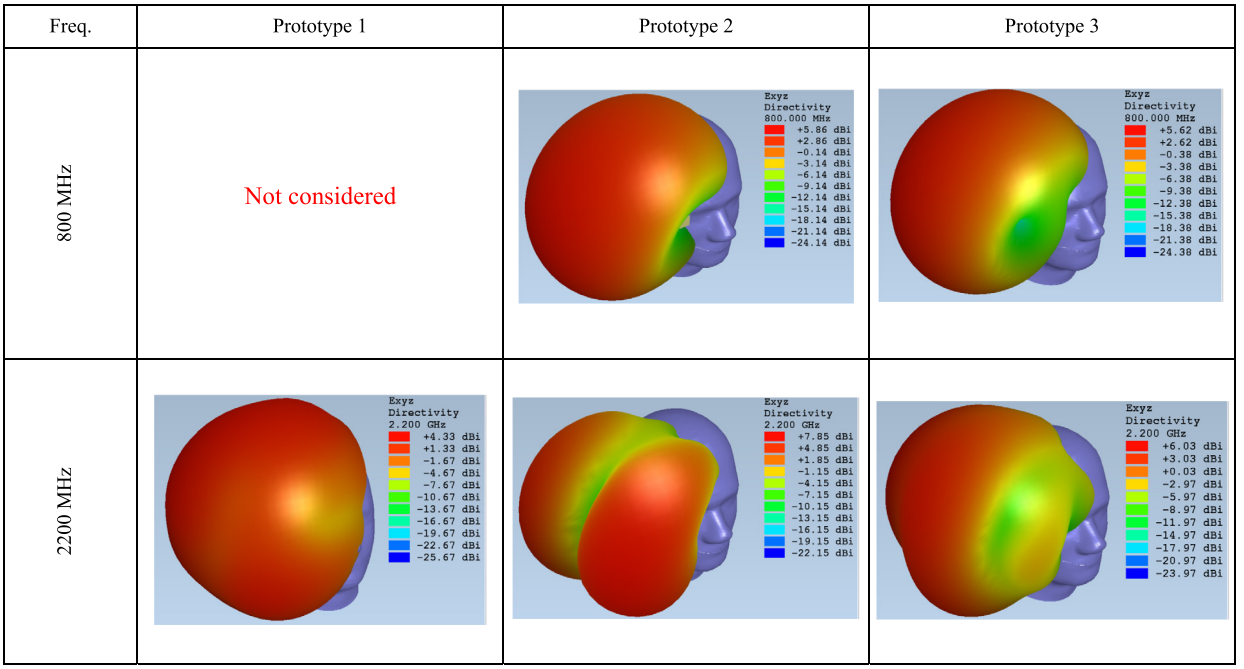

Fig. 4. (Color online.) Simulated radiation patterns at 800 MHz and 2.2 GHz for all three prototypes.

Table 1
Simulated SAR values with SAM phantom (W/kg).

Prototype	Freq. (MHz)	0.25 W Incident power		0.25 W Accepted power (without S_{11})	
		1 g SAR	10 g SAR	1 g SAR	10 g SAR
1	1900	***7.86***	***3.32***	***8.37***	***3.53***
1	2200	***4.31***	***2.07***	***4.88***	***2.35***
1	2500	***4.36***	1.54	***4.39***	1.55
2	835	***4.33***	***2.08***	***4.96***	***2.39***
2	1900	***2.97***	1.47	***3.89***	1.92
2	2200	***4.18***	1.99	***4.54***	***2.16***
2	2500	***3.68***	1.83	***4.69***	***2.33***
3	835	***4.17***	***2.03***	***5.50***	***2.68***
3	1900	***2.47***	1.18	***3.19***	1.53
3	2200	***2.22***	1.04	***2.60***	1.22
3	2500	***1.96***	0.82	***2.11***	0.89

This is more complicated for a real (heterogeneous) head because the latter is composed of several tissue layers, each having different dielectric properties. This layer arrangement creates discontinuities at their interface and sometime resonances in some body parts or organs like the eye for instance: electric fields increase (instead of decreasing, as expected) as we move away from the source. For example, if we expose the eyes to a certain amount of power, the SAR value in the eyes could be twice the SAR value in neighboring tissues, specifically at frequencies like 600 MHz and 2.4 GHz [9,15,16]. It has been also shown that the metallic frames of an eyewear device could act as passive scatters and SAR values in the eyes could significantly increase in this specific case [9].

In this paper, every simulated SAR value have been given for a normalized 0.25 W incident power [14], but it should be mentioned that the incident power in the GSM1800 band should be normalized to 0.125 W if we want our calculations to be realistic.

2.2.1. SAM phantom

Simulated SAR values when the eyewear is placed over a SAM phantom are given in Table 1. They are normalized to an incident power of 0.25 W and an accepted power of 0.25 W (matching not taken into account at the input port in this last case). Liquids with different dielectric properties at different frequencies have been used: $\varepsilon_r = 41.5$; $\tan\delta = 0.467$ at 835 MHz and $\varepsilon_r = 39.2$; $\tan\delta = 0.337$ at 2500 MHz. SAR levels which are above the limits are set in bold italic letters in Table 1. The proximity of the source and the absence of shielding ground plane toward the head are leading to SAR values that are globally much higher than the ones obtained with generic smartphones. It should be also noted that the obtained

Table 2
Simulated SAR values with the VH phantom (W/kg).

Prototype	Freq. (MHz)	Eff. (%)	0.25 W Incident power		0.25 W Accepted power (without S_{11})	
			1 g SAR	10 g SAR	1 g SAR	10 g SAR
1	1900	25.2	***3.53***	1.64	***3.86***	1.79
1	2200	36.0	***2.90***	1.32	***3.04***	1.38
1	2500	42.1	***1.80***	0.85	***1.84***	0.87
2	835	10.0	1.50	0.97	***1.69***	1.09
2	1900	19.8	***1.64***	0.83	***2.03***	1.03
2	2200	21.2	***2.25***	1.09	***2.35***	1.14
2	2500	20.9	***2.51***	1.14	***3.04***	1.38
3	835	12.7	***1.32***	0.80	***1.88***	1.14
3	1900	38.0	***2.40***	0.91	***2.83***	1.07
3	2200	33.3	***2.32***	1.00	***2.82***	1.21
3	2500	37.2	***2.62***	1.01	***2.73***	1.05

radiation efficiencies with our prototypes (10–15% in low band and 20–35% in high band) are largely higher than the ones usually encountered with modern smartphones (radiating with head and hand): 5% in low band and 15% in high band. The 1 g SAR is always above 1.6 W/kg, but simulated values seem to be more acceptable for the 10-g SAR 2 W/kg limit: they are always higher than the limit in low band (except for prototype 1 at 2200 MHz). With prototype 3, SAR values are always lower than those from the other prototypes, because the source is placed further away from the head.

2.2.2. VH phantom

Simulated SAR levels with VH phantom are given in Table 2. The characteristics of the VH tissues simulated with EMPIRE XCcel are dispersive, which means that they are automatically adjusted by the software when frequency sweeps. The obtained SAR values are close to the ones obtained with the SAM head. Especially, the 1-g SAR values are always higher than 1.6 W/kg, but lower than 2 W/kg for the 10-g SAR limit. It should be noted that the heterogeneous VH head has an external geometry which is different from that of the SAM head and therefore, the source/head distance is slightly different from one case to another. Except for prototype 3 at 2500 MHz, SAR values for VH head are always lower than SAR values obtained with SAM head. In our simulation, an interesting phenomenon was observed: the metallic part of the PCB that faces the eye induces an electromagnetic surface wave that propagates in the tissues around the eye. Several SAR distributions are shown for all prototypes (Fig. 5): the maximum SAR always appears on the side of the head with some worrying secondary spots around the eye, especially for prototypes 1 and 3.

2.3. Conclusion on the feasibility study

In this feasibility study, we presented three possible locations for the antennas of 4G wireless eyewear devices operating in the 700–960-MHz and 1.7–2.7-GHz frequency bands. Very good radiation efficiencies have been obtained (10–15% at 835 MHz and 20–35% in high band). In general, SAR values in the head are always higher than the 1-g limit, but lower than the 10-g limit if we consider that the input power is set to 0.25 W. For some prototypes (and some frequencies), SAR peaks are observed in the eye of the user. This feasibility study validates our approach, and we decided to further push our investigations in order to fabricate several prototypes of 3D printed 4G wireless eyewear.

3. Fabricated prototypes

The next step consisted in designing and fabricating realistic eyewear and PCBs. We first selected a standard fabrication process for the PCB where the coupling element is simply printed and the components of the matching network are soldered close to the feeding point of the coupling element. An eyewear design, where one of the branch is replaced by a plastic opening where the PCB can fit, has been developed and fabricated with a 3D printer from ABS plastic material ($\varepsilon_r = 2.97$, $\delta_{loss} = 0.029$). The main idea was to use fast and cheap prototyping techniques. The designed model is presented in Fig. 6. Three holes have been left along the outside part of the ABS branch to let pass the WFL cable (Fig. 7). Three prototypes have been optimized, two of them being very similar to prototypes 2 and 3 previously presented in the feasibility study of this paper. A third mono-band prototype has been designed, where the antenna exhibits a reflection coefficient lower than −6 dB from 700 MHz to 2.7 GHz. In Fig. 8, Dr. Will Whittow wears the plastic eyewear, whereas Fig. 9 shows those eyewear devices placed over a SAM phantom. Three use-cases have been considered: eyewear on the user's head (antenna performances are optimized for this use-case), eyewear on the user's head and finger of the hand touching the touchpad (Fig. 10), eyewear in free space (Fig. 11a). The measurements of the reflection coefficient and of the radiation pattern have been conducted for two of those use-cases (Fig. 11a and b) in a SATIMO chamber.

Prototype 2 has been optimized, placing the coupling element close to the eye, with a 3-component matching network to cover the 700–960-MHz and the 1.7–2.7-GHz frequency bands (Fig. 12). The effect of the finger of the hand of the user

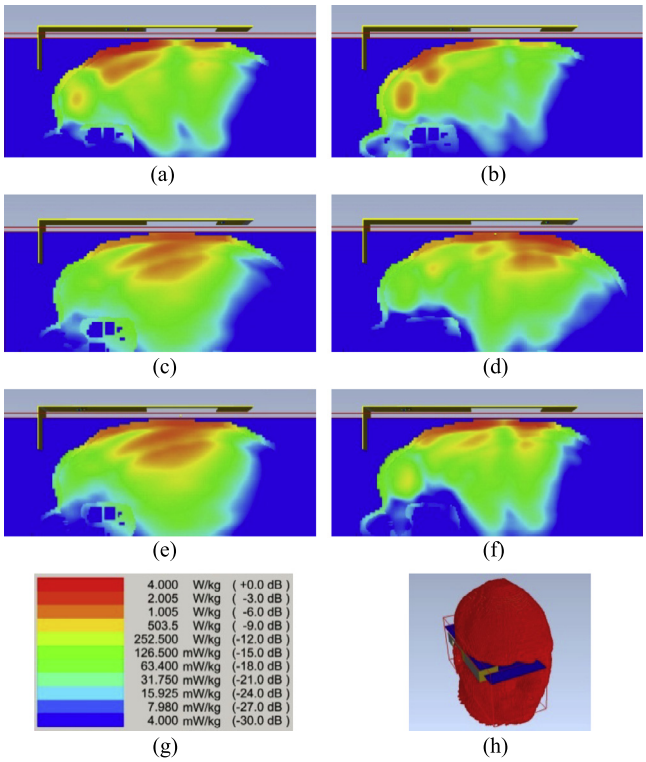

Fig. 5. (Color online.) 1 g SAR distribution simulated for VH (a) prototype 1 at 1900 MHz; (b) prototype 1 at 2500 MHz; (c) prototype 2 at 835 MHz; (d) prototype 2 at 2500 MHz; (e) prototype 3 at 835 MHz and (f) prototype 3 at 2500 MHz; (g) Scale used for every SAR distribution; (h) Horizontal plane in the VH head where the SAR distributions have been extracted.

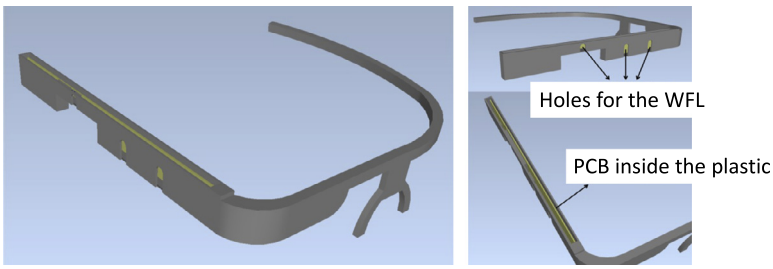

Fig. 6. (Color online.) Simulation model for the 4G wireless eyewear device.

Fig. 7. (Color online.) Eyewear fabricated with a 3D printer.

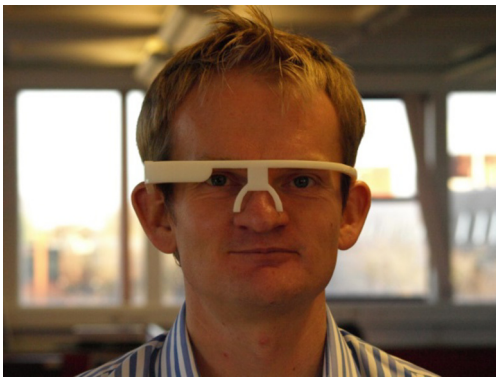

Fig. 8. (Color online.) Eyewear mock-up on the head of a real user.

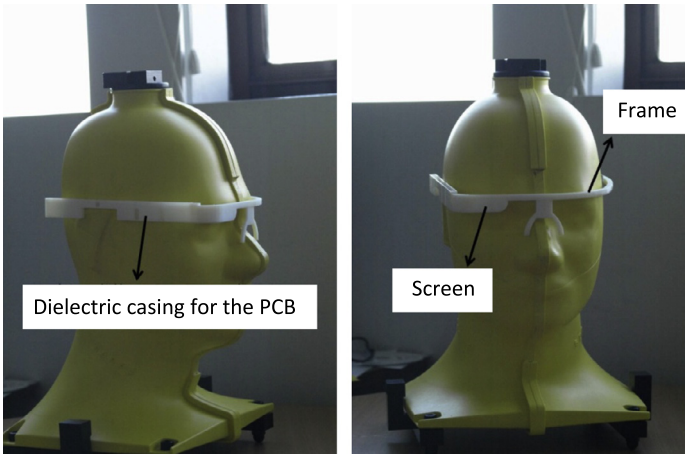

Fig. 9. (Color online.) Eyewear device on a SAM phantom.

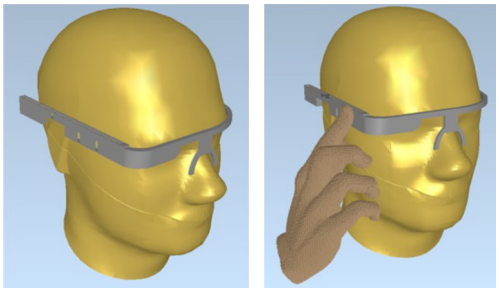

Fig. 10. (Color online.) Eyewear on the SAM phantom for the principal use-case and when the finger is positioned on the touchpad.

over the reflection coefficient can be seen in Fig. 13: it is not negligible in the high band because the finger is placed in the vicinity of the coupling element.

The fabricated PCB is presented in Fig. 14 with ground plane facing (matching network and WFL connector are placed on the other side of the PCB). Simulated and measured reflection coefficients with the SAM head are presented in Fig. 15. The agreement is fair, but the two curves disagree above 2.2 GHz. This difference between simulation and measurement above 2.2 GHz is believed to be due to the frequency-dependent electrical properties of the head liquid, which were modeled as average values ($\varepsilon_r = 40.5$ and $\tan\delta = 0.367$) in the target band for the time-domain simulations.

The efficiency curves in free space and with the SAM head are presented in Fig. 16. With SAM head, the efficiencies range from 9 to 15% in the low band and 20 to 35% in the high band, showing also a good compliance with simulations.

Prototype 3 has been optimized when placing the coupling element between the ear and the eye with a 3-component matching network to cover the 700–960-MHz and 1.7–2.7-GHz frequency bands (Fig. 17). The effect of the finger upon the reflection coefficient can be seen in Fig. 18. It is almost negligible in the high band. Simulated and measured reflection coefficients with the SAM head are presented in Fig. 19. The agreement is fair, but the two curves disagree above 2.2 GHz

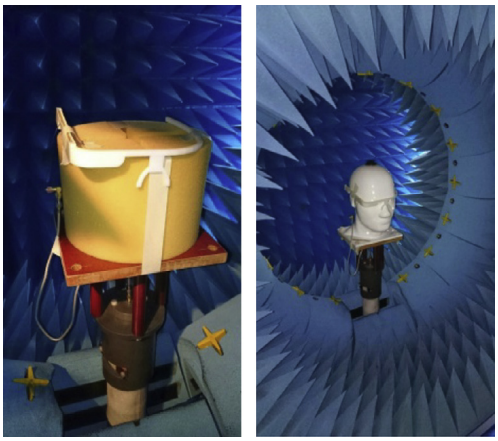

(a) (b)

Fig. 11. (Color online.) Eyewear device placed in a SATIMO facility for reflection coefficient and radiation pattern measurements: (a) eyewear device over a foam support for free-space use; (b) eyewear device over a SAM head (principal use-case).

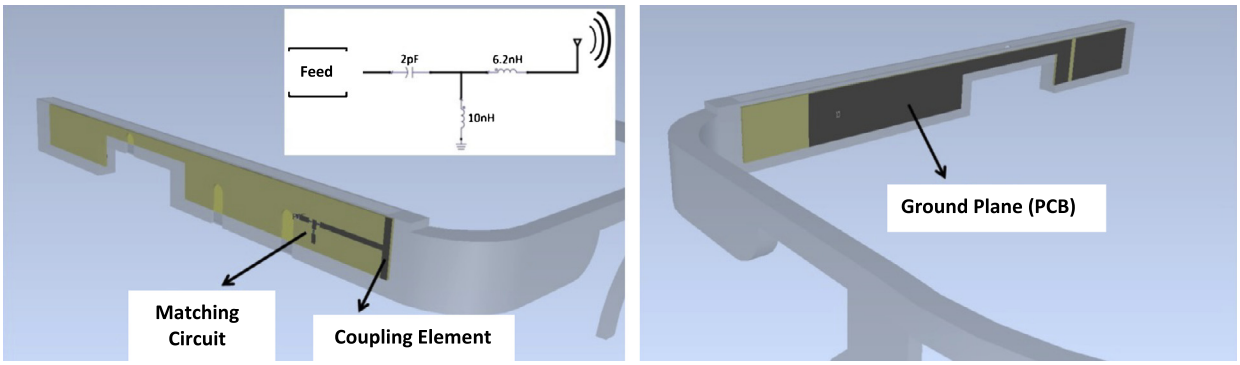

Fig. 12. (Color online.) Prototype 2.

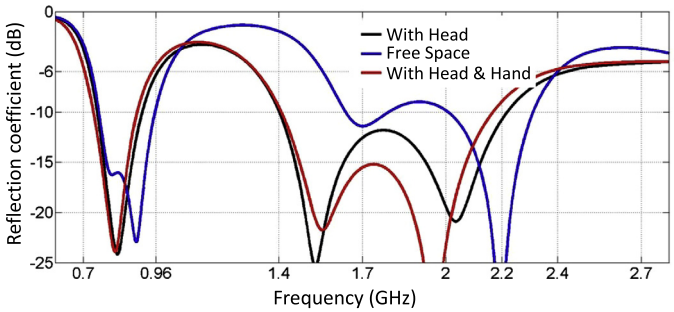

Fig. 13. (Color online.) Reflection coefficient of prototype 2 for all three use-cases.

Fig. 14. (Color online.) PCB for prototype 2.

due to the frequency-dependent electrical properties of the head liquid in reality. The efficiency curves in free space and with the SAM head are presented in Fig. 20. With the SAM head, the efficiencies range from 7 to 12% in the low band and 9 to 18% in the high band.

Novel mono-band prototype 1 has been optimized placing the coupling element behind the ear with a 3-component matching network to operate continuously from 700 to 2700 MHz (Fig. 21). The effect of the finger of the hand of the user

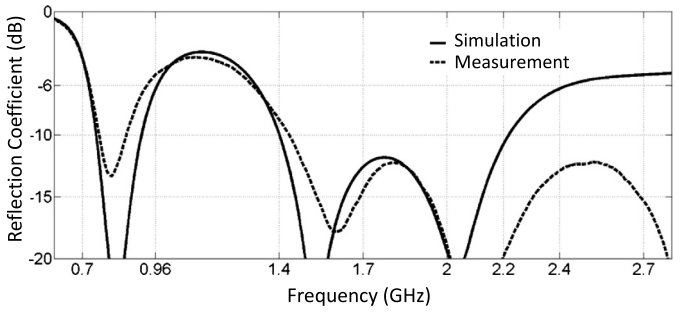

Fig. 15. Simulated and measured reflection coefficient of prototype 2 with the SAM head.

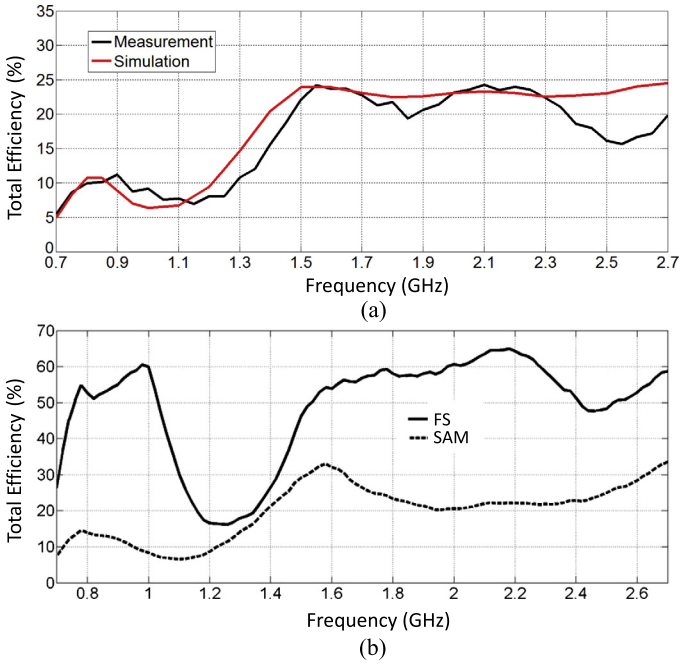

Fig. 16. (Color online.) (a) Comparison of simulated and measured efficiencies with the SAM head; (b) Measured efficiency for prototype 2 in free space (FS) and with the SAM head (SAM).

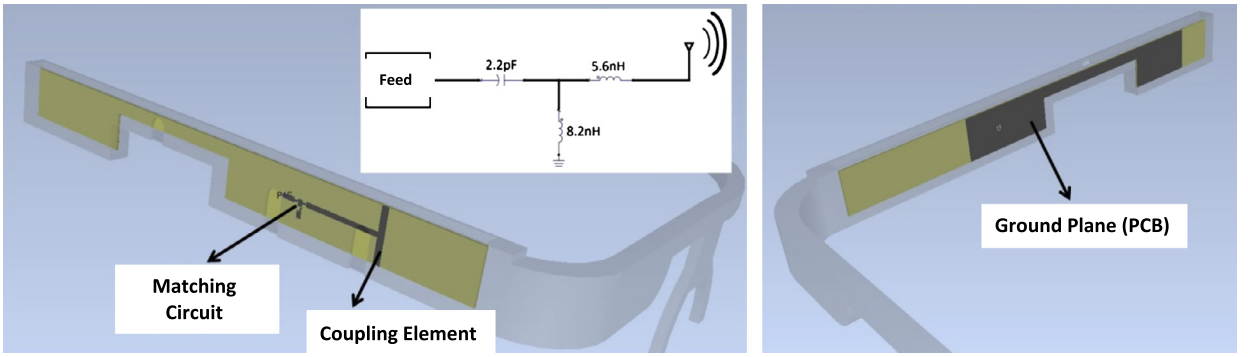

Fig. 17. (Color online.) Prototype 3.

upon the reflection coefficient is shown in Fig. 22. The fabricated PCB is shown in Fig. 23, where the coupling element is shown with its matching network and the very small WFL connector. Simulated and measured reflection coefficients with SAM head are presented in Fig. 24. The agreement is fair but the two curves disagree above 2.2 GHz. The efficiency curves in free space and with the SAM head are presented in Fig. 25. With SAM head, the efficiencies range from 15 to 16% in the low band and 16 to 21% in the high band.

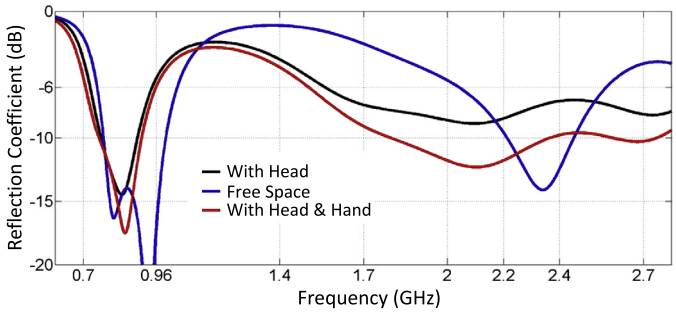

Fig. 18. (Color online.) Reflection coefficient of prototype 3 for all three use-case.

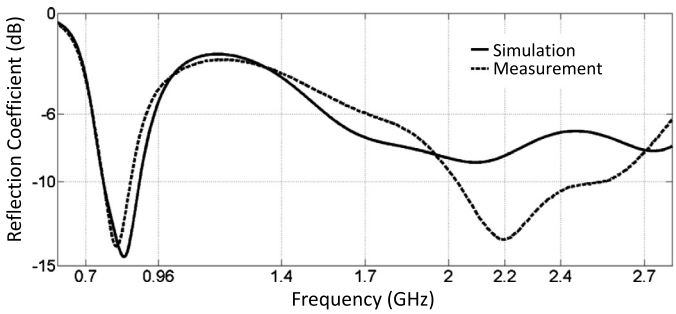

Fig. 19. Simulated and measured reflection coefficient of prototype 3 with SAM head.

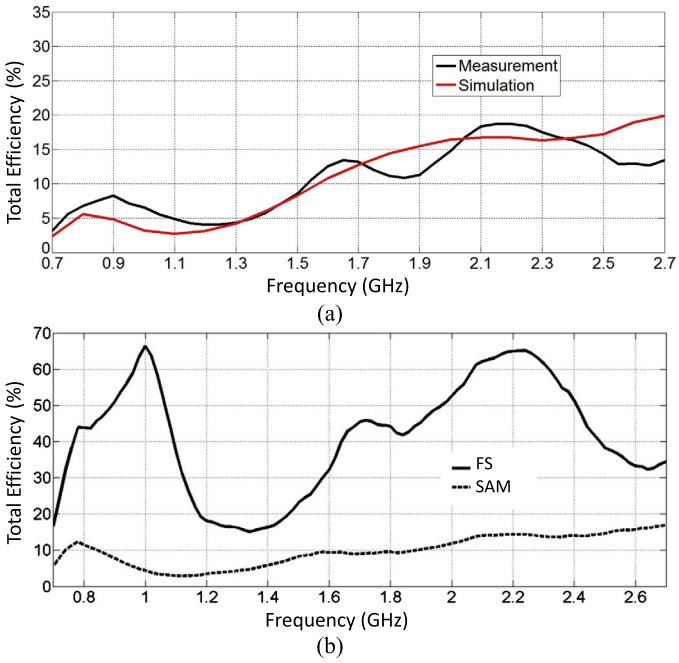

Fig. 20. (Color online.) (a) Comparison of simulated and measured efficiency with SAM head; (b) measured efficiency for prototype 3 in free space (FS) and with the SAM head (SAM).

For prototype 1, we achieved several reflection coefficient measurements when the eyewear was placed on real human users (Fig. 26). Two of those measurements are shown in Fig. 27 (two different users): they are very similar and stay below −6 dB from 700 to 2700 MHz. The agreement with the simulated reflection coefficient of the eyewear device placed over the SAM head is fair but not fully compliant.

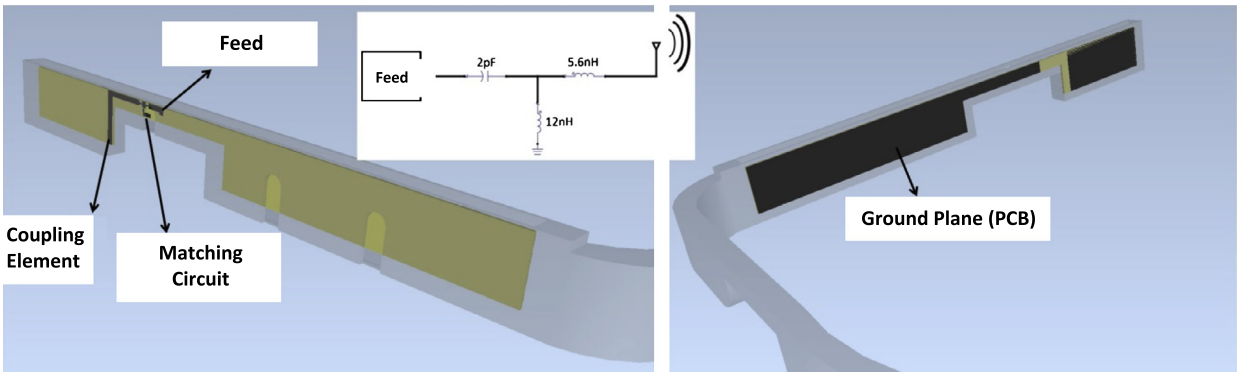

Fig. 21. (Color online.) Prototype 1.

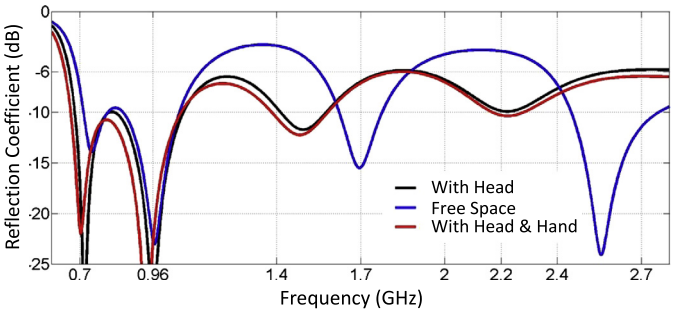

Fig. 22. (Color online.) Reflection coefficient of prototype 3 for all three use-cases.

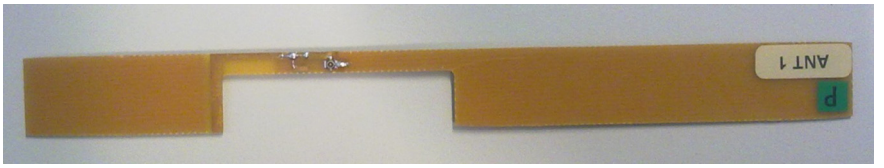

Fig. 23. (Color online.) PCB for prototype 1.

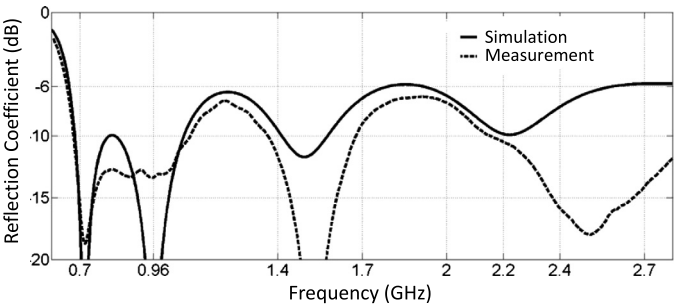

Fig. 24. Simulated and measured reflection coefficient of prototype 1 with SAM head.

In Fig. 28, we show two reflection coefficients measured with a short and a long WFL cable (calibration is done until the end of those cables, therefore taking into account their losses). The two measurement results are generally in agreement, although some ripples are seen for the measurement with a long cable.

SAR simulations have been also done with those new prototypes. Behaviors similar to the ones found in the feasibility study have been evidenced: 1-g SAR values are higher than the limit and 10-g SAR values are lower than the limit. The cut-plane where the SAR values are extracted is presented in Fig. 29a and one of the results obtained at 700 MHz is shown in Fig. 29b (not normalized). A strong distribution of the E-field is found close to the eye of the user.

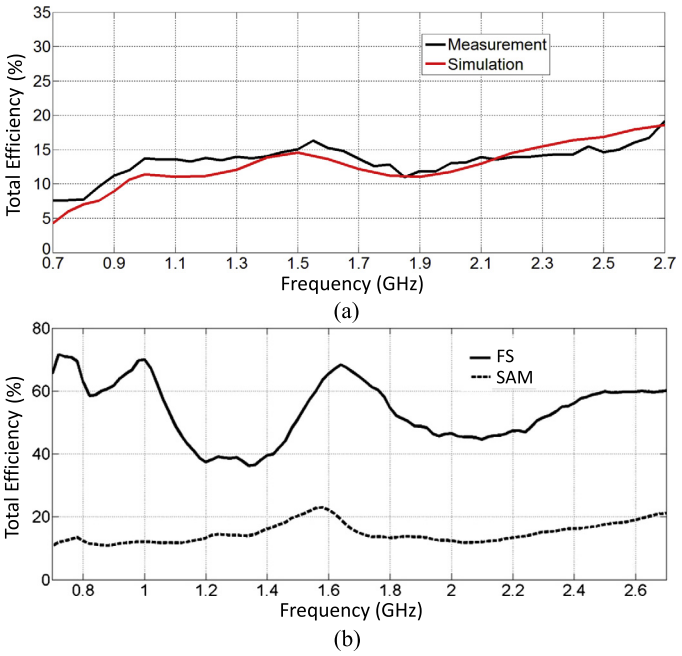

Fig. 25. (Color online.) (a) Comparison of simulated and measured efficiency with the SAM head; (b) measured efficiency for prototype 1 in free space (FS) and with the SAM head (SAM).

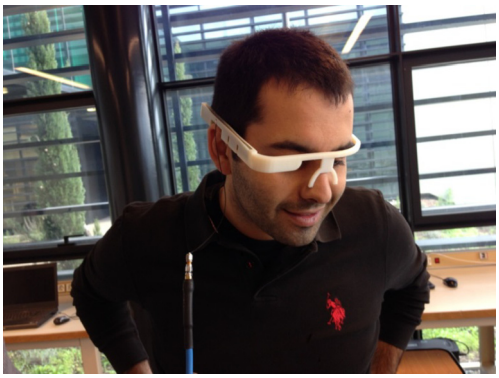

Fig. 26. (Color online.) Measured reflection coefficient of prototype 1 with a real user.

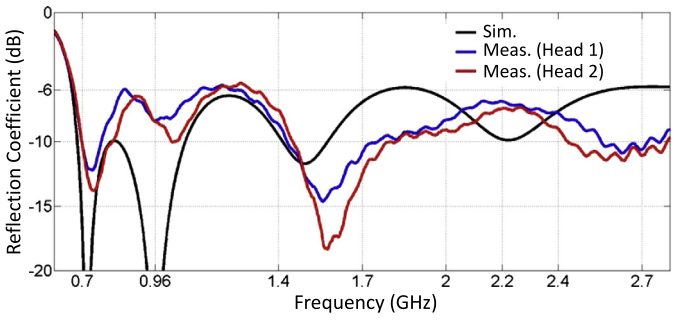

Fig. 27. (Color online.) Measured reflection coefficient of prototype 1 for two different real users. Simulated curve is obtained with eyewear place over the SAM head.

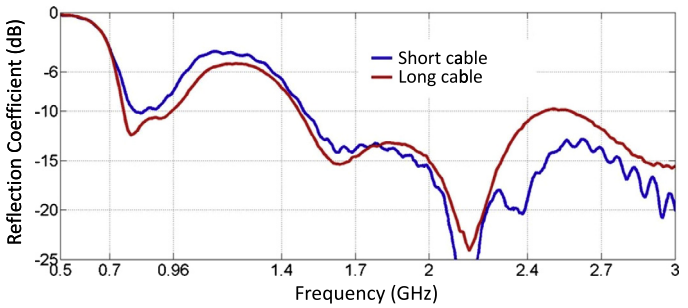

Fig. 28. (Color online.) Measured reflection coefficient of prototype 1 with a short and with a long WFL cable.

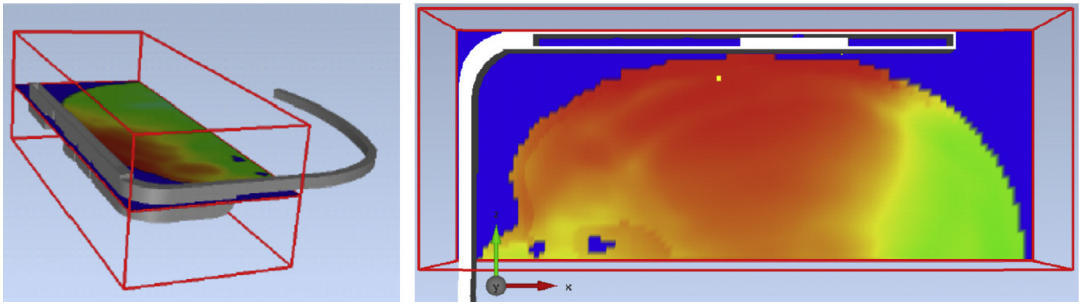

(a) (b)

Fig. 29. (Color online.) 1-g SAR simulated distribution in a VH head at 700 MHz for one of the prototypes.

4. Conclusion

In this paper, we presented a feasibility study to design 4G antennas (700–960 MHz and 1.7–2.7 GHz) for eyewear devices. Eyewear can be connected to last-generation cellular networks, Wireless Local Area Networks or wireless hotspots. Three coupling element type antennas supplied by a matching network have been evaluated in terms of reflection coefficient and total radiation efficiency when the eyewear is placed on the user's head. We also presented SAR simulations when the eyewear device is positioned over a homogeneous SAM phantom and over a heterogeneous VH phantom: the SAR levels were compared to international limit values. In a second step, we presented experimental results obtained with 3D printed eyewear and coupling elements etched on classical PCB substrate where the matching circuits are optimized close to the feeding point of the coupling element. Simulated and measured values are in very good agreement: 7 to 16% and 9 to 35% of total efficiency are respectively obtained for the low- and high-frequency bands. However, simulated SAR values are somewhat higher than authorized limits with preoccupant high electromagnetic field distribution close to the eye of the user. From our best knowledge, this is the first time that such a work is performed on wireless eyewear. However, in the future, SAR reduction techniques should be studied to be compliant with the international limits. We also plan to start additional studies about eyewear with metallic frames and also the possibility to achieve MIMO (Multiple-Input–Multiple-Output) communications when integrating a second PCB and associated coupling element in the other branch of the frame.

Acknowledgements

The authors thank COST VISTA 1102 for support, CREMANT for measurements, Frédéric Devillers for the fabrication of antenna supports, Joe Wiart for the loan of the SAM head and hand.

References

[1] http://www.google.com/glass/start/.
[2] H. Jidhage, A. Stjernman, Hooked loop antenna concept for bluetooth headset applications, in: Proc. IEEE Antennas and Propagation Conference 2004, AP-S 2004, July 2004, pp. 3521–3524.
[3] J.-H. Chou, S.-W. Su, Matching a bluetooth headset antenna on a small system ground by using a conductive wire, Microw. Opt. Technol. Lett. 51 (12) (2009) 2802–2805.
[4] K.-L. Wong, M.-R. Hsu, W.-Y. Li, S.-W. Su, A. Chen, Study of the bluetooth headset antenna with the user's head, Microw. Opt. Technol. Lett. 49 (1) (2007) 19–23.
[5] J. Anguera, A. Andújar, C. Picher, L. González, C. Puente, S. Kahng, Behavior of several antenna topologies near the human head at the 2.4–2.5 GHz band, Microw. Opt. Technol. Lett. 54 (8) (2012) 1911–1916.

[6] A. Cihangir, W.G. Whittow, C.J. Panagamuwa, F. Ferrero, G. Jacquemod, F. Gianesello, C. Luxey, Feasibility study of 4G cellular antennas for eyewear communicating devices, IEEE Antennas Wirel. Propag. Lett. 12 (2013) 1704–1707.
[7] P. Vainikainen, J. Ollikainen, O. Kivekas, I. Kelander, Resonator-based analysis of the combination of mobile handset antenna and chassis, IEEE Trans. Antennas Propag. 50 (10) (2002) 1433–1444.
[8] G. Bellanca, G. Caniato, A. Giovannelli, P. Olivo, S. Trillo, Effect of field enhancement due to the coupling between a cellular phone and metallic eyeglasses, Microw. Opt. Technol. Lett. 48 (1) (2006) 63–65.
[9] W.G. Whittow, R.M. Edwards, A study of changes to specific absorption rates in the human eye close to perfectly conducting spectacles within the radio frequency range 1.5 to 3.0 GHz, IEEE Trans. Antennas Propag. 52 (12) (2004) 3207–3212.
[10] http://www.optenni.com/.
[11] IEC, Human exposure to radio frequency fields from hand-held and body-mounted wireless communication devices—human models, instrumentation, and procedures—part 1: procedure to determine the specific absorption rate (SAR) for hand-Held devices used in close proximity to the ear (frequency range of 300 MHz to 3 GHz), IEC 62209-1:2005, 2005.
[12] IEEE, IEEE recommended practice for determining the peak spatial-average specific absorption rate (SAR) in the human head from wireless devices: measurement techniques, IEEE Std 1528, 2003.
[13] B. Beard, et al., Comparisons of computed mobile phone induced SAR in the SAM phantom to that in anatomically correct models of the human head, IEEE Trans. Electromagn. Compat. 48 (2) (2006) 397–407.
[14] M. Siegbahn, et al., An international interlaboratory comparison of mobile phone SAR calculation with CAD-based models, IEEE Trans. Antennas Propag. 52 (4) (2010) 804–811.
[15] V. Singh, A. Qusba, A. Roy, R.A. Castro, K. Mcclure, R. Dai, R.J. Greenberg, J.D. Weiland, M.S. Humayun, G. Lazzi, Specific absorption rate and current densities in the human eye and head induced by the telemetry link of an epiretinal prosthesis, IEEE Trans. Antennas Propag. 57 (10) (2009) 3110–3118.
[16] W.G. Whittow, C.J. Panagamuwa, R.M. Edwards, J.C. Vardaxoglou, On the effects of straight metallic jewelery on the specific absorption rates resulting from face-illuminating radio communication devices at popular cellular frequencies, Phys. Med. Biol. 53 (2008) 1167–1182.